ATOMIC AND MOLECULAR DYNAMICS IN INTENSE OPTICAL FIELDS[1]

B. Sheehy and L. F. DiMauro

Chemistry Department, Brookhaven National Laboratory, Upton, New York 11973

ABSTRACT

The unprecedented high intensities made accessible by the development of ultra-
short pulse laser systems have uncovered a host of new phenomena and changed
the way that we think about atomic and molecular dynamics. We review these
developments in the context of some of the basic models that have evolved to
explain them. The successes and limitations of simple semiclassical models of
strong-field atomic phenomena are discussed. Photodissociation dynamics have
shown a rich complexity in strong fields—bond softening, above-threshold dis-
sociation, coulomb explosion—which we review. The promise of the new laser
systems in the field of coherent control of molecular dynamics is also discussed.

INTRODUCTION

The development of short-pulse laser technology in recent years has opened a
new domain of exploration in physical chemistry: Optical intensities are now
attainable such that the optical electric field strength is comparable to, or even
exceeds, the Coulomb-binding fields in molecules and atoms. Perturbative tech-
niques are wholly inadequate in dealing with the new phenomena uncovered in
this regime, and there have been many innovative approaches to the daunting
theoretical problems involved. Although a great deal remains to be understood,
some surprisingly simple pictures have evolved, which go a long way toward un-
derstanding the basic physics of atomic and molecular interactions with strong

---

[1]The US Government has the right to retain a nonexclusive royalty-free license in and to any
copyright covering this paper.

optical fields. We hope to convey these ideas in the context of reviewing the major developments of the gas-phase chemistry in the strong-field regime.

It is simpler to consider first the dynamics of an atom in a short, intense laser pulse, as many of the molecular phenomena have close parallels. In this highly nonlinear regime, an electron bound to an atom or molecule may in general absorb multiple photons [multiphoton absorption (MPI)], sometimes even more than are energetically required to exceed the ionization threshold [above-threshold ionization (ATI)]. ATI is manifested in the photoelectron energy spectrum as a series of peaks separated by the photon energy and was first observed by Agostini et al (1). The multiphoton absorption might also be followed by the radiative decay of the electron back to the atomic or molecular ground state, resulting in the emission of a more energetic photon, whose frequency is an odd harmonic of the exciting field. This process is known as optical harmonic generation (OHG).

A third possibility is that multiple electrons may be removed, either simultaneously (correlated process) or sequentially. The possibility of a correlated process motivated a great deal of early atomic MPI work (see Reference 2 for a discussion). Although early experimental observations thought to be evidence of such a process were later explained as higher-order sequential processes, recent observations (3, 4) confirm the existence of nonsequential multiple ionization in noble gases.

A simple picture connecting all three phenomena—ATI, OHG, and nonsequential ionization—has evolved (5, 6, 7) that considers the physics in the limit of optical fields large enough that the removal of the first electron proceeds by simple field ionization. In this limit, the instantaneous Stark potential near the peak of the optical cycle suppresses the Coulomb barrier sufficiently that the electron in the ground state may tunnel through it in a time short compared with an optical period. Following this bound-free transition, the evolution of the electron is determined solely by the oscillating electric field until, after approximately one half of an optical cycle, it returns to the vicinity of the atomic core. There are then three possible interactions with the core upon return: radiative decay back to the ground state, elastic scattering, or inelastic scattering. In the model, these three interactions are related to, respectively, OHG, ATI (in the energy and angular distributions of the photoelectrons), and nonsequential ionization. In the first section of this review, we explore these connections and discuss their limitations.

In intense field molecular photodissociation, singly and multiply ionized fragments are produced with considerable energies. Frasinski et al (8) initially proposed that these large energies arose from a rapid stripping of the electrons from the molecule, which proceeded via field ionization, followed by the mutual repulsion of the ionic fragments left behind. This direct excitation into

the continuum at small internuclear separation has been termed a Coulomb explosion. If all of the electrons are removed in a time short compared with a time characteristic of the evolution of the nuclear wave functions, the kinetic energy of the ion fragments should be equal to the Coulombic potential energy of point particles, with the appropriate charge, that are separated by the equilibrium internuclear distances. The observed fragment energies are, however, considerably lower. Frasinski et al (8) proposed that the sequential removal of the electrons occurs as the molecule is dissociating, and the lower observed kinetic energies reveal the dynamics of the dissociation on a femtosecond time scale. A powerful technique, covariance mapping (9), allows one to identify the fragments arising from different dissociation channels, and in the field-ionization model, the energy of each fragment reveals the internuclear distance at which the dissociation occured.

There is some controversy surrounding this picture of the Coulomb explosion. Much of it centers on the time scales involved for field ionization, for nuclear motion, and for field-induced states of the electrons. Pulses with rise times that are fast compared with the nuclear vibrational period would be expected to produce fragments whose total experimentally observed kinetic energy E_{exp} was nearly equal to the Coulomb energy E_c of the fragments separated by the equilibrium internuclear distance R_e (10). In pulses with longer rise times, fragmentation would occur at larger internuclear distances, yielding lower total kinetic energy. Furthermore, one would expect E_{exp}/E_c to be lower in fragmentation channels involving higher charge states because the nuclei should move farther apart during the removal of more electrons. There are some discrepancies in the experimental record, but it seems clear that the dependence of the total kinetic energy on both pulse width and charge state of the fragments is much less than one would expect in the field-ionization model.

In any event, there is every reason to expect that the dynamics involved in the Coulomb explosion are richer, since nothing precludes the effects already observed in the photodissociation of H_2^+ from occurring in the case of other molecules. These effects are best understood by considering the problem in terms of molecular states dressed by the laser field. In the absence of any radiative coupling, the dressed states are just product states of the molecular eigenstates and the photon number states of the laser field. To each bare molecular state corresponds a ladder of diabatic potential curves, each identical to the zero-field potential curve but shifted by an integer multiple of the photon energy. In Figure 1 these curves are shown for the $1s\sigma_g$ and $2p\sigma_u$ states of H_2^+, where the label n refers to the number of photons removed from the laser field. The light couples these states and distorts the potential curves; by diagonalizing the Hamiltonian, the adiabatic potential curves shown in Figure 1 are obtained. Much of the photodissociation physics may be understood in terms of these
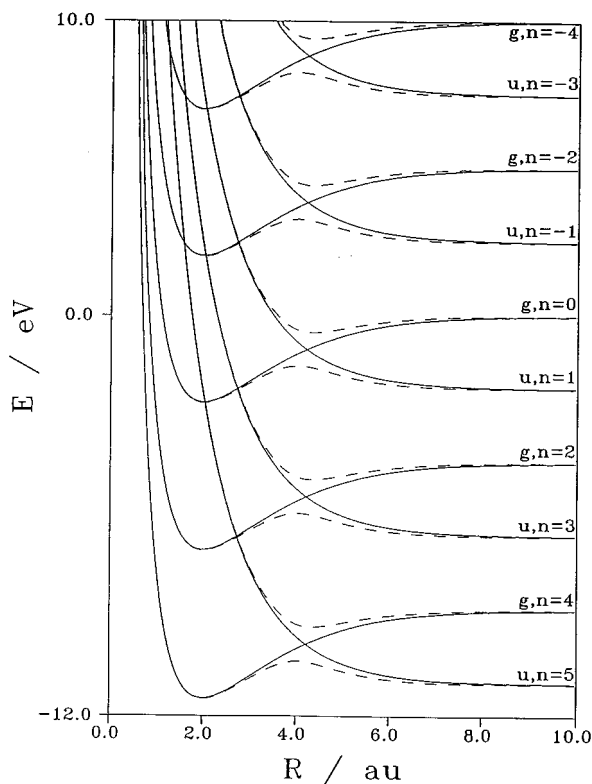
Figure 1   Potential energy curves for the $1s\sigma_g$ and $2p\sigma_u$ states of H_2^+. The solid lines represent 10 diabatic states: bare molecular states dressed by $n = \pm 5$ photons. The dotted curves represent the adiabatic potentials, obtained by diagonalizing the Hamiltonian, including the length-gauge radiative coupling between 60 diabatic states. The optical parameters are $\lambda = 532$ nm and $I = 1.5 \times 10^{13}$ W/cm^2.

level repulsions. For example, bond softening occurs when level repulsion suppresses the ground state barrier below the energy of an occupied vibrational state (11, 12). Above-threshold dissociation may be understood in terms of constraints on the system to move diabatically or adiabatically through particular anticrossings. At higher fields than those shown in Figure 1, wells that are deep enough to support bound states can form in the adiabatic potentials at large internuclear separation. Since these light-induced states exist only when the light intensity is within a limited range, the population can become "trapped" there as the laser pulse reaches this intensity range, and be stable against dissociation until the intensity is again out of this range. There is evidence (13)

that this vibrational trapping occurs in the photodissociation of H_2^+, and it may also be an important factor in Coulomb explosion dynamics (10, 14–19).

In a later section of this article, we review the work on bond softening, above-threshold dissociation, and vibrational trapping as it developed in studies of the hydrogen molecular ion. Following this, we consider Coulomb explosion dynamics.

An experimenter's optical control over chemical dynamics is usually limited to frequency tuning around optical resonances. Short-pulse technology promises to extend the control of photochemistry beyond tunability and employ the coherence properties of light to obtain quantum state selectivity within a manifold of degenerate states. There are two principal approaches to this coherent control. Multiple pulses of different frequencies with well-defined phase relationships may be employed to create quantum interferences, controllable through the relative phase. Another, and in principle much more flexible, method tailors the modulation and spectral content of a pulse to optimally drive the desired transition. This is sometimes called optimal control (20), and it typically exploits the broad spectral bandwidth of short pulses. Chirped-pulse amplification, a technique used to generate short, intense pulses, requires the temporal stretching of a pulse prior to amplification. In this stretching, the spectral composition of the pulse is expanded spatially, affording an opportunity to selectively attenuate or shift in phase selected spectral components. In this way, one can effectively tailor the pulse in frequency space. One has considerable freedom in shaping the pulse, and modulation periods on the femtosecond scale may be obtained in the final amplified and recompressed pulse. We briefly review the multiple frequency approach below. For pulse shaping, the reader is referred to Reference 21, and the work cited therein.

ATOMS IN STRONG OPTICAL FIELDS

The rescattering model introduced above assumes that the peak optical field strength is sufficiently large that an electron may tunnel through the Coulomb barrier in a time short compared with the optical period. This condition may be quantified, in terms of the field-free binding energy of the electron E_0 and the frequency and intensity of the ac field, by the Keldysh nonadiabaticity parameter γ,

$$\gamma = \frac{\omega_L}{\omega_{\text{tun}}} = \sqrt{\frac{E_0}{2U_p}},$$

where ω_L is the angular frequency of the optical field, ω_{tun} is the tunneling rate through the barrier at the peak of the optical field, and U_p is the "ponderomotive potential." U_p is equal to the time-averaged kinetic energy of a free

electron oscillating in an ac field of intensity I. In atomic units, it is given by $U_p = I/4\omega_L^2$. For $\gamma \ll 1$, the tunneling approximation is valid, and this condition is often referred to as the tunneling regime. In the multiphoton regime, $\gamma > 1$, nonresonant and resonant multiphoton couplings contribute more to the ionization rate than tunneling does. ATI, OHG, and nonsequential ionization are also observed in the multiphoton regime.

A justification for the tunneling or multiphoton distinction may be seen in Figure 2, which compares the multiphoton ionization yield data by Walker et al (3) for helium irradiated by a 160-fs, 780-nm laser pulse with two theoretical calculations. The time-dependent calculation labeled TDSE-SAE is based on a difference equation approximation to the time-dependent Schrödinger equation (TDSE) in the single-active electron (SAE) approximation (3, 22). The SAE approximation considers a single electron moving in the potential created by the nucleus and the remaining electrons of the atom, which are frozen in their ground state orbitals. Also shown (short dashed line) is a calculation based on the work of Amnosov, Delone, and Krainov (ADK) (23) that accounts only for tunneling ionization. The SAE calculation fits the data very well; ADK clearly underestimates the rate at low intensities, where multiphoton processes are important.
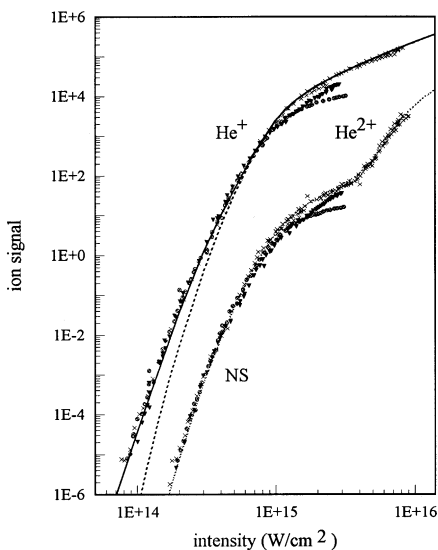

Figure 2   Measured He ion yield for linearly polarized 160-fs, 780-nm light. Theoretical calculations are shown in the solid (TDSE-SAE) and dashed (ADK) curves. The dotted line through the He^{2+} low-intensity data represents the single ionization ADK rate multiplied by a constant.
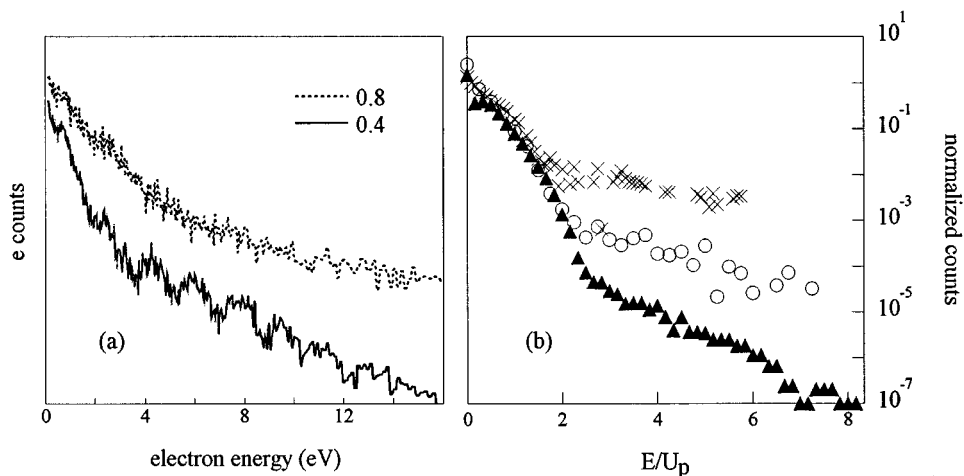
Figure 3   Helium photoelectron spectra for linearly polarized 160-fs, 780-nm light. (*a*) The ATI structure diminishes as the intensity is increased from 0.4 to 0.8 PW/cm^2. (*b*) Scaled spectra, E/U_p at 0.2 ($\times$), 0.4 ($\circ$), and 1.0($\triangle$) PW/cm^2.

Another distinction between the two regimes may be seen in the difference in the helium photoelectron energy distributions, shown in Figure 3. At 0.4 PW/cm^2, $\gamma = 0.7$, there is clear ATI structure. Further into the tunneling regime, at 0.8 PW/cm^2, $\gamma = 0.5$, the spectrum is structureless. Though both multiphoton and tunneling processes produce modulations in the energy spectrum with a period equal to the photon energy in a homogeneous optical field, the tunneling contributions from regions of different intensity in the laser pulse are shifted in energy, and this washes out the modulations in the tunneling case. This is not the case for contributions to the multiphoton ionization signal from different intensity regions because of a first-order cancellation of ponderomotive shifts and the ac Stark shift of intermediate states (for a discussion of these effects, see Reference 2). The loss of structure is thus a good empirical indicator of a transition from the multiphoton to the tunneling regime.

Figure 3*b*, in which the electron energies are plotted in units of the ponderomotive potential, illustrates another feature of the photoelectron spectrum related to the dynamics of tunneling ionization. Consider the classical motion in the optical field of an electron that tunnels from the core near the peak of the optical field. It oscillates in the field, with an average drift velocity determined by the phase of the optical field at which it tunneled through the Coulomb barrier. The maximum drift energy that the electron may acquire is $2U_p$. Consistent with this "Simpleman" model, the figure shows that almost all of the

electrons fall between 0 and $2U_p$. Also consistent is the decrease in the fraction of electrons above $2U_p$ with increasing intensity, as the interaction moves from the multiphoton to the tunneling regime. The model fails, however, to account for the presence of electrons above $2U_p$, even at the highest intensities, where the tunneling approximation should be valid. These electrons may arise from a rescattering of the tunneling electron off of the ion core as it is returned to the core by the oscillating optical electric field (6, 7). The electron's motion relative to the optical phase is shifted by the interaction with the core, and it may then acquire more energy from the optical field—up to $10U_p$.

Perhaps the most striking success of the simple rescattering model is to be found in the behavior of harmonic generation. The photon energy distribution in the production of high harmonics is characteristically a nearly flat distribution that extends out to an intensity-dependent cutoff energy, where the yield falls off rapidly (24). Expressed in terms of the ponderomotive potential and binding energy, this cutoff occurs (25) at $3.2U_p + E_0$. In the rescattering model, this is also the maximum energy with which an electron, escaping by tunneling and subsequently accelerated in the optical field, returns to the core approximately one-half optical cycle later. The interpretation is straightforward: In order to radiatively decay back to the ground state, the electron must return to the core, and the maximum return energy is reflected in the maximum energy of the photon produced.

The angular distribution of photoelectrons in strong fields also shows characteristics that suggest electron return to the core and a subsequent interaction. When energy-resolved angular distributions are measured in xenon (26), a pronounced peak away from the axis defined by the optical polarization vector appears at an energy that varies linearly with intensity. Because of the azimuthal symmetry about the optical polarization vector, the distribution is a ring. When the electron energy is normalized to the intensity-dependent ponderomotive potential, the rings appear between $8U_p$ and $10U_p$, independent of intensity. In the classical rescattering model, if an electron accelerated back to the core scatters elastically, reverses its velocity, and is accelerated again in the optical field, the final kinetic energy distribution both peaks and cuts off at $10U_p$. A purely classical model certainly oversimplifies the phenomenon: The electron wave function undergoes significant transverse spreading before it returns to the core, and the elastic scattering must be treated quantum-mechanically. Core structure must also be considered, as the strength of the effect varies in other noble gases.

However, there is strong theoretical support for associating these rings with back-scattered electrons, as the rescattering model suggests. Lewenstein et al (27), modeling the core with a short-range potential and using the strong-field

approximation, made a quasiclassical calculation, which allows the separate analysis of contributions to the photoelectron spectrum arising from different classical trajectories. In the strong-field limit in which the calculations were done, electrons with energies above $6U_p$ originated predominantly from back-scattering off of the core. Schafer & Kulander (28), using the TDSE-SAE calculations mentioned above to take "snapshots" of the wave function at different times in a model laser pulse, observed the electron wave function amplitude growing at a distance from the core (associated with tunneling), and a strong interference as this piece of the wave function evolved back to the origin approximately one half of an optical cycle later. They were also able to calculate the ring structure (26), and their results for xenon are shown in Figure 4, in comparison with the experimental data. The calculations at other intensities reproduce the $8U_p$–$10U_p$ scaling. The theoretical curve in the figure is much sharper, as it includes no averaging over the spatial and temporal laser pulse profile.

It seems natural to extend the rescattering model and consider inelastic scattering of the returning electron as a model for correlated two-electron emission. The debate over the existence of a direct, correlated multiple-ionization process as opposed to simple sequential ionization has an interesting history. It was first believed to occur in alkaline earth atoms, but this proved to be the case only
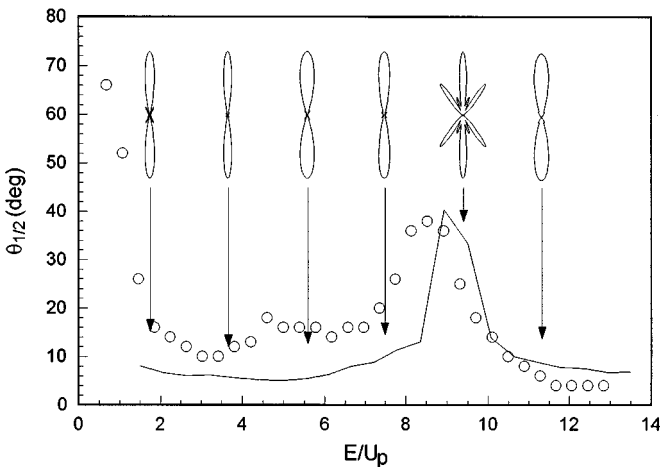

Figure 4 Scattering rings in xenon: $\theta_{1/2}$, the angle from the light polarization axis within which one half of the photoelectrons are emitted, vs the scaled electron energy E/U_p. The solid lines and polar plots represent the results of the TDSE-SAE calculation. The peak at zero energy in the experimental data ($\circ$) is due to ponderomotive scattering off of the spatially inhomogeneous laser pulse. Optical parameters: $\lambda = 1\ \mu$m, $I = 30\,$TW/cm^2, 50 ps FWHM pulsewidth.

under somewhat exotic conditions, for example, when a doubly excited state with large angular momentum, a "planetary double Rydberg state," could be excited as an intermediate state (29). These states are exceptional in that the decay of doubly excited autoionizing states to the double continuum is usually slower than the decay to excited ionic states. In the latter case, while doubly excited intermediate states play a role, the ionization itself is sequential. In the short-pulse ionization of xenon, there are two rates present in the production of Xe^{2+} as a function of peak laser intensity (30), and their presence was long believed to be evidence of a direct double ionization, until it was shown (31, 32) that a sequential path through an excited ionic state explained the double rate. A more complete and detailed review of this topic may be found in Reference 2; we have outlined it here only to put the approach of the rescattering model in context.

In helium, a double rate is also seen in the intensity dependence of the He^{2+} yield (3, 31, 33). Unlike xenon, however, the ionization occurs in the tunneling regime at an intensity where there are no excited bound states in helium, thereby eliminating the resonance mechanism that occurs in xenon as a possible explanation. The He^{2+} yield obtained by Walker et al (3) is shown with the He^+ yield in Figure 2. As the photoionization process saturates with increasing intensity, the yield curve turns over, and the yield increases only slowly as the volume of the laser focus above saturation intensity grows. Note that the low-intensity process for the production of He^{2+} saturates at the same intensity as the production of He^+. This finding was verified in detail (3) by repeating the measurement with progressively larger focal spot sizes while maintaining a fixed volume imaged by the detector. This procedure increases the change in slope of the yield curve at saturation and allows precise identification of the saturation intensity. That the low-intensity double ionization shuts off as the density of the neutral in the interaction volume is dropping and the density of the singly charged ion is growing implies that there is a direct, or nonsequential, double ionization of the neutral. At higher intensities, where the slope of the He^{2+} yield curve again increases, the sequential process is important, and it eventually saturates as well.

Not only is the doubly charged ion formed directly from the neutral, but the yield is clearly proportional to the rate of formation of He^+ by tunneling ionization. In Figure 5, the ratio of double to single ionization yields is plotted as a function of intensity. The solid curve is the ratio of two theoretically calculated rates of He^+ production, multiplied by a constant α. The TDSE-SAE calculation accurately predicts the yield over the full intensity range and includes both tunneling and multiphoton processes. The ADK calculation includes only tunneling ionization and accurately reproduces the data at high intensities. The ratio of the ADK to TDSE-SAE rates is then the fraction of single ionization
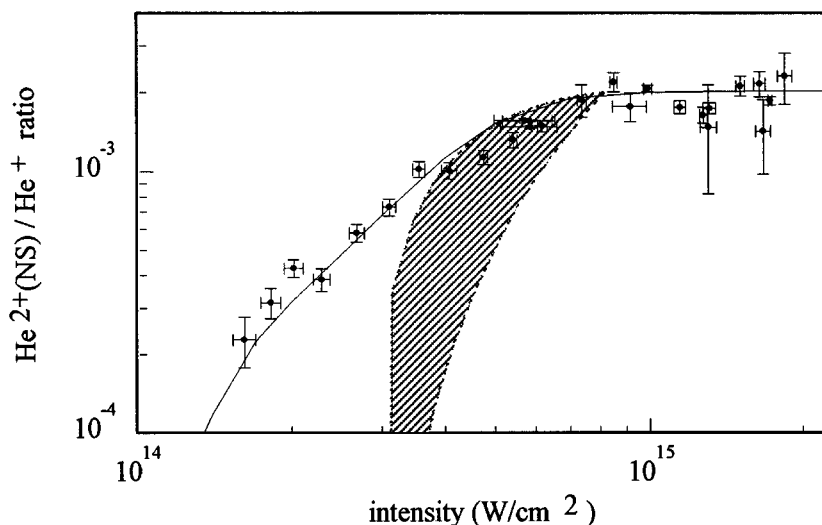
Figure 5 Intensity dependence of the He^{2+}/He^+ yield ratio. The theoretical (*solid*) line is explained in the text. The shaded region indicates the expected range of the double ionization cutoff in the classical rescattering model

that proceeds by tunneling. The constant α is the experimentally obtained ratio of He^{2+} to He^+ at the saturation intensity. The close agreement between the solid curve and the measured ratio of He^{2+} to He^+ production strongly suggests that the nonsequential double ionization is related to the tunneling ionization of the neutral.

Corkum (7) used a rescattering model in which a tunneling electron returns to the core and collisionally ionizes the second electron to fit helium double-ionization yield data. The fit parameter is the spreading of the electron wave packet that occurs during the approximately one-half optical cycle between the tunneling and the return to the core. He estimated the wave packet spread at $3a_0/fs$ (where a_0 is the Bohr radius), which implies a spread of $3a_0$–$4a_0$ at the time that the electron returns to the core. However, the TDSE-SAE calculations, which accurately reproduce all of the single-electron dynamics, give a wave packet spread at return of $30a_0$–$40a_0$ (3). The latter value is also consistent with the spreading of a simple Gaussian wave packet, whose transverse dimension at the time of tunneling is the core diameter. The upper limit on the He^{2+}/He^+ yield attributable to inelastic scattering is then 1.5×10^{-4} at the He^+ saturation intensity, which is over an order of magnitude less than the experimentally observed value of 2×10^{-3} (3).

The rescattering model also predicts that the double ionization will have a low-intensity threshold that is not observed experimentally. The maximum energy of the returning electron is only sufficient to remove the second electron from helium when $3.2U_p > 54.4\,\text{eV}$. For the experimental conditions of Figures 2 and 5, this corresponds to an intensity of $0.3\,\text{PW/cm}^2$. If one requires only that the returning electron promote the He^+ to an excited state, which would then quickly ionize in the laser field, the threshold is $0.23\,\text{PW/cm}^2$. The data, which extend down to $0.14\,\text{PW/cm}^2$, show no evidence of either threshold.

Fittinghoff et al (33) proposed an alternative explanation of the nonsequential double ionization that is consistent with its connection to tunneling ionization in the neutral, known as shakeoff. If the first electron is removed from the neutral atom quickly enough that the remaining electron does not adiabatically adjust to the loss of screening, there will be some amplitude of the second electron wave function in excited states of the ionic potential, or in the continuum. Any population in an excited ionic state would quickly ionize in the laser field. Shakeoff has been observed in synchrotron experiments in which a single energetic photon ionizes helium (34). Though plausible, quantitative predictions based on shakeoff are difficult, failing a complete two-electron quantum calculation.

One challenge to the shakeoff hypothesis is posed by the observed polarization dependence of the nonsequential process. The ellipticity dependences of both the single- and double-ionization yields are shown in Figure 6 for two
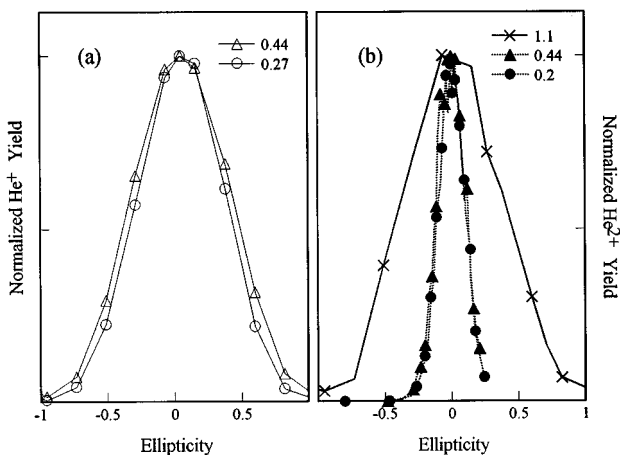

Figure 6   Ellipticity dependence for (*a*) He^+ and (*b*) He^{2+} yields at different intensities ($\lambda = 780\,\text{nm}$). The values $-1, 0, 1$ correspond to right circular, linear, and left circular polarization. Intensities are shown in PW/cm^2.

intensities. At the higher intensity, the double ionization is dominated by the sequential process, and the ellipticity dependence is approximately the same as that of the singly charged ion yield. At lower intensities where the He^{2+} is produced nonsequentially, the double-ionization yield falls off very quickly with the introduction of even a slight ellipticity. This finding is consistent with the rescattering model, since any acquired angular momentum would cause the tunneling electron to miss the core. The effect on the shakeoff hypothesis is unclear: Shakeoff may be thought of as a scattering event between the two electrons during the ejection of one of them. Walker et al (3) suggest that additional angular momentum in the outgoing electron may reduce the strength of its interaction with the second electron, thereby reducing the yield.

STRONG-FIELD PHYSICS OF PHOTODISSOCIATION

Like short-pulse atomic dynamics, the physics of short-pulse molecular dynamics divides into a weak-field and strong-field limit. The issues of the weak-field limit arise from the complexity introduced by the added degrees of freedom in the molecule. The treatment of the optical interaction is still perturbative, however, and the role of the light is still essentially driving transitions between states of the bare molecular system or bound states and the continuum; these transitions can be described in terms of unperturbed Franck-Condon factors. As the optical fields grow larger ($I > 10^{11} \, W/cm^2$), resonances induced by the light itself arise. These may be considered in a number of ways. In this review we consider first the time-independent treatment of field and molecule together in terms of dressed states. As mentioned in the introduction, this gives a good basic understanding of the physics of bond softening, above-threshold dissociation, and vibrational trapping. Results of time-dependent calculations are discussed, but for a discussion of the techniques, the reader is referred to a recent review by Giusti-Suzor et al (35). The development will be as it applies to H_2^+, since that system is both the simplest and the most studied.

The tunneling approximation has also been applied in the molecular case. The field ionization model of Coulomb explosion photodissociation considers this limit. It and the role of more complex dynamics in the Coulomb explosion are discussed in the section on Coulomb Explosion.

Photodissociation of H_2^+

The fragmentation of H_2^+ may be treated as principally involving only two electronic states: the attractive $1s\sigma_g$ ground state and the first repulsive $2p\sigma_u$ state. In all of the experiments to date, the preparation of the H_2^+ has been done with the same laser pulse that accomplishes the dissociation. Photoelectron spectra in long-pulse experiments (11, 12, 36) have shown that the molecular

ion is formed in vibrational levels of the $1s\sigma_g$ state. The energy distribution of the dissociation fragments indicates that dissociation to the $2p\sigma_u$ is the main dissociation path in the long-pulse regime. That the ionization and dissociation are sequential has also been demonstrated experimentally (12, 36, 37).

The time-independent theory may be formulated in two ways, which yield essentially the same result. In the generalized Floquet approach (38, 39), the optical field is treated classically, and a Fourier expansion of the radiative coupling and molecular eigenfunctions is made. Alternatively, the field may be treated quantally, in terms of the photon number states $|N-n\rangle$, where N is the very large initial number of photons in the field, and n represents the number of photons absorbed. The molecular eigenfunction in the product representation, with the restriction to two bare molecular states, is then

$$\psi(r, R, N, E) = \sum |N - n\rangle\phi_g F_{n,g}(R, E) + |N - n\rangle\phi_u F_{n,u}(R, E),$$

where the $\phi_i(r, R)$ ($i = g, u$) are the field-free electron wave functions for the $1s\sigma_g$ and $2p\sigma_u$ states in the Bohr-Oppenheimer approximation, and the functions $F_{n,i}(R, E)$ ($i = g, u$) are the nuclear wave functions. The Hamiltonian is given by the sum of three terms that represent the bare molecule, the radiation field, and the coupling between them.

$$H = H_0 + H_{rad} + V_{int}.$$

In the limit $V_{int} = 0$, one obtains the eigenvalues represented by the solid lines in Figure 1. In this diabatic, or dressed-channel basis, the potential curves are identical to those of the bare molecule but shifted in energy by the amount $-n\hbar\omega$.

Before diagonalizing to obtain the adiabatic basis, a gauge must be chosen for the dipole coupling term V_{int}. If all states were included in the calculation, the results would of course be independent of gauge. In the Coulomb gauge, $V_{int} = (e/Mc)\mathbf{p} \cdot \mathbf{A}$, the large values of the dipole moment at small internuclear distances make the restriction to two states unjustified. Comparison of results obtained with variational calculations by Muller (40) have demonstrated that the two-state approximation is justified in the length gauge ($V_{int} = e\mathbf{r} \cdot \mathbf{E}$). For time-dependent calculations of short-pulse interactions, the divergence of the dipole moment at large internuclear separations, which is a problem in the length gauge, is avoided because the interaction is over before large separations are reached.

By truncating the infinite set of states and diagonalizing, one obtains the adiabatic states, whose eigenvalues as a function of R are shown by the dashed curves in Figure 1. Convergence is reached using a small number of states around $n = 0$; for an intensity of 10^{13} W/cm^2, including ± 5 photon states is sufficient (41).
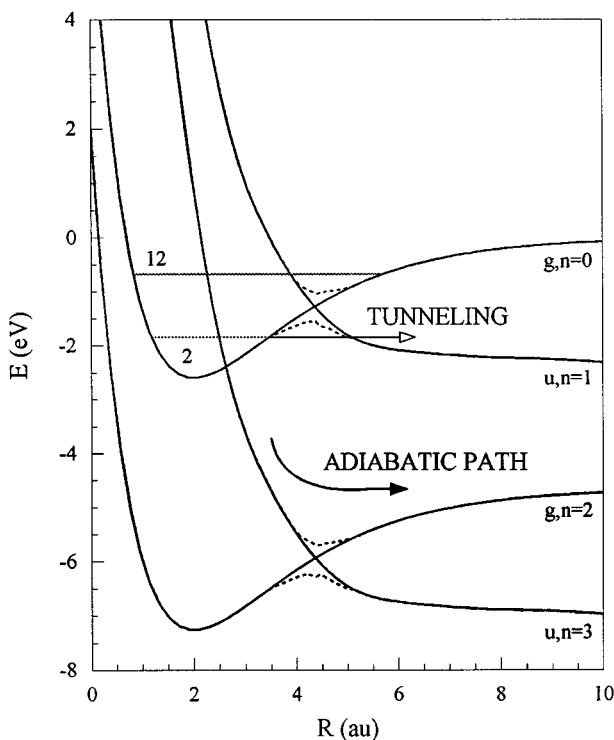
Figure 7   Potential energy curves for the $1s\sigma_g$ and $2p\sigma_u$ states of H_2^+, showing possible dissociation paths. See text for details.

In Figure 7, the diabatic and adiabatic curves are shown on an expanded vertical scale to illustrate the dynamics of the dissociation. The calculations shown are for the second YAG harmonic, $\lambda = 532$ nm, at an intensity of 10^{13} W/cm^2. As the intensity is increased, the barrier in the ground state (g, $n = 0$) potential curve is progressively lowered. Dissociation may occur along the u, $n = 1$ potential curve, with a net absorption of one photon, for population originating in vibrational levels above or just below the top of the barrier, the latter escaping by tunneling through the barrier. At higher intensities, even the $v = 1$ and $v = 2$ levels eventually become unbound. Because of the gradual weakening of the binding potential, this process has been named bond softening (11).

One can see in Figure 7 that, paradoxically, at low intensities a higher-order process can dominate a low-order process. Population in the lower vibrational states of the g, $n = 0$ channel may dissociate along the one-photon u, $n = 1$ path

only by tunneling through a relatively large barrier. A more probable path is a diabatic transition to the u, $n = 3$ channel, which entails the absorption of three photons, followed by either a diabatic or adiabatic passage through the gap at the u, $n = 3$ and g, $n = 2$ anticrossing. As that gap opens up, the adiabatic path becomes the more probable; the system dissociates along the g, $n = 2$ channel, which involves the stimulated emission of one photon back into the laser field. The total process is thus fourth order—a three-photon absorption followed by one-photon emission—although the net absorption is only two photons. This process is known as above-threshold dissociation (ATD), by analogy to the excess absorption of photons beyond the ionization limit (ATI) in atoms (1, 11).

The experimental implication is that, at low intensities, given an initial population distributed among the lower vibrational levels of the ground state, ATD will be the dominant dissociation mechanism. As the intensity is increased and the barrier is lowered, eventually even low vibrational levels will dissociate via bond softening, thereby shutting off the higher-order ATD channel. Such an unusual channel closure is in fact observed experimentally (see below).

Higher vibrational states, above $v = 8$ for the conditions of Figure 7, which would be unbound in the absence of the u, $n = 1$ channel, may in fact be stabilized against photodissociation; they may be "trapped" in the adiabatic potential well formed by the avoided crossing. This effect has been calculated at several wavelengths (42–46). Light-induced bound states similar to these trapped states have been described for cw laser fields at fixed intensity (47–49). In Figure 7, the trapping is most effective for higher vibrational levels, which are more difficult to populate, but the intensity at which the well forms and the ground state vibrational levels that will be trapped, are a function of the wavelength. Lower v states, which are experimentally accessible, may also be trapped (see below).

The photodissociation of H_2^+ has been studied at numerous wavelengths, mostly in the long-pulse regime (> 1 ps). There are a few experimental details that apply to nearly all of the experiments. Typically, the laser is focused into an ultra-high vacuum system into which neutral hydrogen is leaked. The H_2^+ is prepared by the same laser pulse that dissociates it. The energies of the electrons and ion fragments produced are measured by time-of-flight spectrometry. For ion collection, a small dc electric field is applied in the interaction region, parallel to the detection axis. The laser polarization is oriented parallel to this axis, so ion emission in the forward (toward the detector) and backward (away from the detector) directions is symmetric. The dc field reverses the velocity of those fragments emitted in the backward direction, and the time delay between their arrival at the detector and the arrival time of the forward ions provides a measure of the ion energy at the time of dissociation.

In the long-pulse regime, the energy spectrum of the photoelectrons produced in the ionization of the neutral provides the initial vibrational distribution of the H_2^+. For shorter pulses, the photoelectron spectrum is complicated by intermediate Rydberg states that are shifted in and out of resonance, depending on the instantaneous light intensity, by the ac Stark effect. In a short pulse, the shifts of both the intermediate states and the ionization threshold are approximately equal, and that, in conjunction with the propensity rule $\triangle v = 0$, washes out the vibrational information in the photoelectron energy spectrum. In the long pulse, the photoelecron acquires yet another energy shift from the ponderomotive acceleration that it experiences as it leave the laser focus. This shift is approximately equal in magnitude to the Stark shifts of the intermediate Rydberg states and the ionization potential, and restores vibrational information to the photoelectron energy spectrum. These resonances due to Stark-shifted intermediate states are similar to those observed in short-pulse atomic multiphoton ionization (50). They have been observed in other diatomics (51) as well as H_2^+ (52).

Figure 8 shows the photoelectron spectrum of H_2 irradiated with the second harmonics from Nd:YAG (532 nm) and Nd:YLF (527 nm), taken from the work of Yang et al (36). Ionization of the neutral molecule requires a minimum of seven photons at these wavelengths ($h\nu = 2.3$ eV), and peaks corresponding to seven- and eight-photon (ATI) absorption are visible. The vibrational structure of the H_2^+ $^1\Sigma_g^+$ ion is clearly resolved. At the lowest intensities, the vibrational level distribution is accurately predicted by the Franck-Condon factors for nonresonant absorption. As the intensity increases, however, the shift toward predominantly $v^+ = 0$ occupation indicates the presence of an intermediate resonant state. By varying the intensity at both wavelengths, it was determined that the primary intermediate state is H_2 $J^1\Delta_g(v = 0)$, with a lesser contribution from H_2 $I^1\Pi_g(v = 0)$. Although this means that, at some laser-pulse energies, the vibrational distribution in dissociation experiments is not constant over the interaction volume, in practice it is possible to determine sufficiently the initial vibrational level distribution of the H_2^+ before dissociation. Another feature to note in Figure 8 is the gradual suppression of the lowest-energy peaks in the spectra as intensity increases. This effect, common in strong-field atomic photoionization, demonstrates the ponderomotive shift of the ionization threshold to higher energy. As the intensity increases, the seventh photon has insufficient energy to ionize the neutral and leave the ion in the higher-lying vibrational levels, and these channels close off. The energy at which the peak occurs is unchanged, since the energy acquired by ponderomotive acceleration is equal to the shift of the ionization threshold.

Vibrational distributions derived from Figure 8 are used to calculate the proton energy spectra shown by the solid curve in Figure 9. The numbers by each peak indicate the initial vibrational level. The dashed curve shows the experimental proton energy spectrum, with two broad peaks. The proton energy of the first peak corresponds to the one-photon bond softening dissociation; slightly less than one-half photon energy higher lies the two-photon dissociation, or ATD, peak. The theoretical curve is obtained using the peak laser intensity, without any spatial or temporal averaging over the pulse (35). The theory seems to underestimate the amount of ATD from the $v > 2$ levels, but the agreement is quite good. The distribution of initial vibrational levels is also responsible for the fact that the spacing between the two experimental peaks is
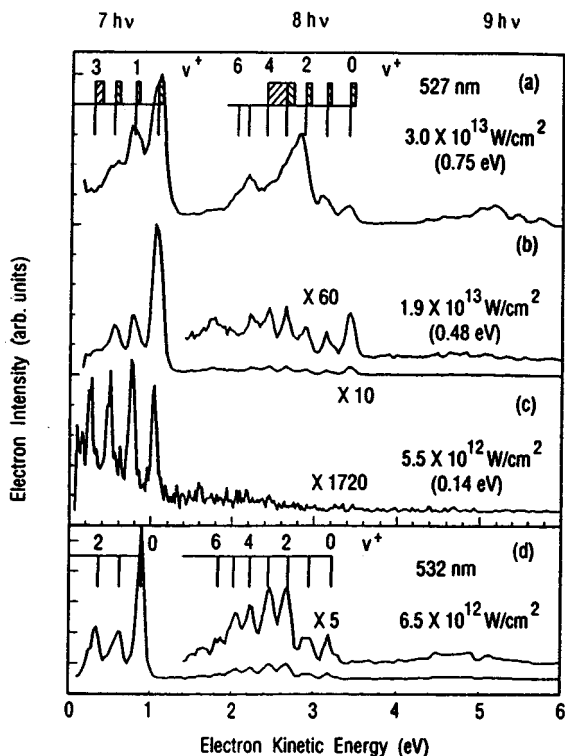

Figure 8 Photoelectron spectra of the H_2 molecule at several intensities of 527- and 532-nm light. The tick marks indicate the unperturbed vibrational levels of the H_2^+ molecular ion ground state. The numbers in parentheses are the ponderomotive potentials U_p at each intensity.
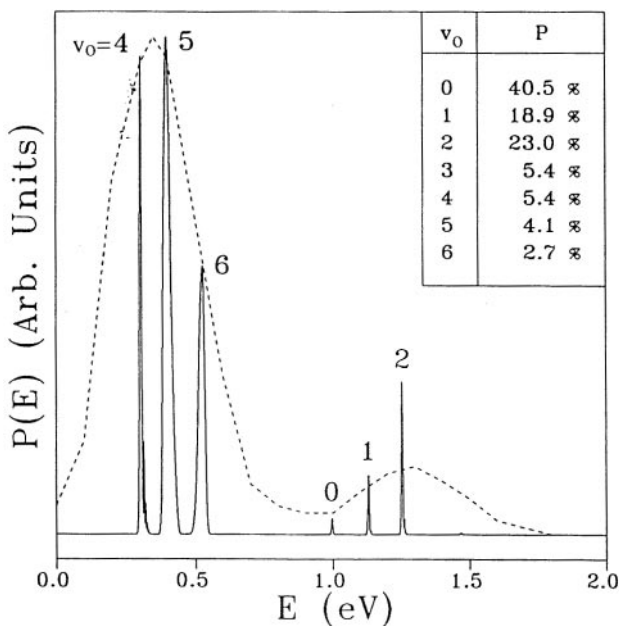
Figure 9 Calculated (*solid line*) and experimental (*dotted line*) proton energy spectrum from the dissociation of H_2^+ with 532 nm, $1.0 \pm 0.5 \times 10^{13}$ W/cm^2 light. The theoretical curve was calculated for an intensity of 1.45×10^{13} W/cm^2, with a vibrational distribution derived from the experimental photoelectron spectrum (Figure 8*d*).

less than the $0.5\,h\nu$ that one would expect if all of the ions originated from a single vibrational level.

Both the two-photon and three-photon ATD peaks can be seen on a log scale in the spectrum displayed in Figure 10, from Bucksbaum et al (11). The proton angular distributions are also shown, from which one can infer that the molecule is rotated into alignment with the laser polarization. At the lowest intensity shown, where the dissociation rate is low, the highly peaked distributions demonstrate that the molecules that do dissociate are those that are oriented parallel to the laser polarization. The higher intensity shown is above the point where nearly all of the molecules in the interaction volume dissociate, and the angular distribution remains highly peaked, implying that the laser field aligns the molecules before or during the dissociation. Normand et al (37) performed a more complete experimental demonstration and detailed study of this alignment on the CO molecule by using two orthogonally polarized laser pulses with a variable delay betweem them.

The intensity dependence of the branching ratios between dissociation channels is displayed in Figure 11 for 532-nm radiation (36). The total fraction of fragmentation into both ATD channels is increasing with intensity, in apparent contradiction to the channel closure argument given above. This increase may be due to an intensity dependence or saturation of the population of the upper vibrational levels of the ion, which would dissociate via the one-photon channel. The ratio of three-photon to two-photon dissociation decreases with increasing intensity. This is to be expected, as the gap between the g, $n = 2$ and u, $n = 3$ channels in Figure 7 increases with intensity, making the passage along the adiabatic path more likely.

At 769 nm, in an intensity window at $\approx 10^{14}$ W/cm^2, the light-induced well in the adiabatic $2p\sigma_u$ curve occurs at energies degenerate with low-lying
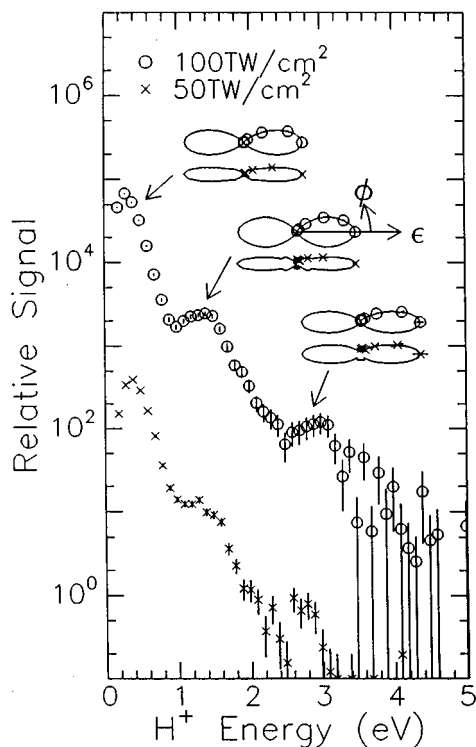
Figure 10 Proton kinetic energy and angular distributions measured at $\lambda = 532$ nm, with 50 TW/cm^2 ($\times$) and 100 TW/cm^2 ($\circ$) intensities. The lowest energy peak indicates bond softening, while the peaks at 1.5 and 3 eV are ATD channels. [From Bucksbaum et al (11).]
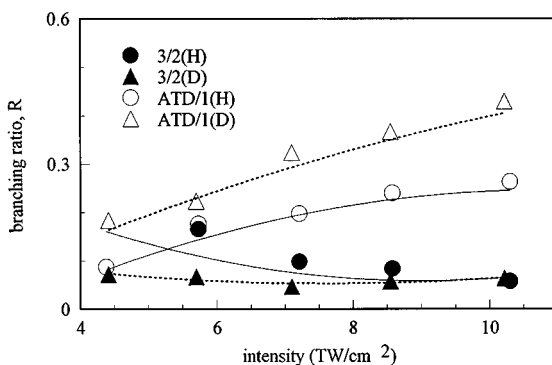
Figure 11   Intensity dependence of the ATD branching ratios R of H_2^+ and D_2^+ at $\lambda = 532$ nm. Open symbols represent the ratio of total ATD yield to bond softening, solid symbols represent the ratio of three-photon to two-photon dissociation.

vibrational levels in the $1s\sigma_g$ state. If the intensity remains within this range for an appreciable time during the laser pulse, there may be population transfer into the adiabatic well. Experimental proton energy spectra from the work of Zavriyev et al (13) for a 160 fs pulse is shown in Figure 12. At low intensities, one sees again a bond-softening and ATD peak (the bond-softening peak is not visible at the intensities shown but does occur at lower intensities), but as the intensity increases, most of the ion yield goes into a broad peak at higher energies. Zavriyev et al found that the structure in this high-energy peak is consistent with dissociative ionization from bound vibrational levels in the adiabatic well to the repulsive $2p\sigma_u$ state. The Franck-Condon overlaps for these transitions are shown above the spectra in the figure. Interestingly, the pulse length is critical to populating these levels. Their proposed scenario, illustrated in Figure 13, considers the system in a particular vibrational level of the $1s\sigma_g$ state classically moving between its outer and inner turning points. Considering the rise of the pulse, the ion would first reach its outer turning point 15 fs after its formation, when the intensity is $\approx 3 \times 10^{13}$ W/cm^2. At this intensity, the one-photon gap to the $2p\sigma_u$, $n = -1$ state is very large, and a transition is very unlikely, so the ion turns around and executes another vibrational cycle. The ion passes the three-photon gap to the $2p\sigma_u$, $n = -3$ state approximately 40 fs after its formation, when the intensity is $\approx 9 \times 10^{13}$ W/cm^2. There is a significant probability at this intensity that the system will cross the gap diabatically, to the $2p\sigma_u$ curve. In the time it takes to reach the new outer turning point and return, however, the gap has opened up more, and the system is now trapped in the adiabatic well.

The identification of the structure on the high-energy proton peak with trapping in the three-photon adiabatic well is still somewhat controversial. Time-dependent calculations by Yao & Chu (43, 44) predict this trapping in the three-photon well for a 100-fs, 775-nm pulse. However, their calculations freeze the rotational degrees of freedom. Aubanel et al (46) included rotational excitation and found that it destroyed the trapping in the three-photon well, but that trapping of higher vibrational levels in a well that formed in the $2p\sigma_u$, $n = -1$ state was robust.

The presence of light-induced bound states may stabilize a molecule through the most intense part of a laser pulse, leaving a significant probability that the molecule will survive, at least until the point on the trailing edge of the pulse
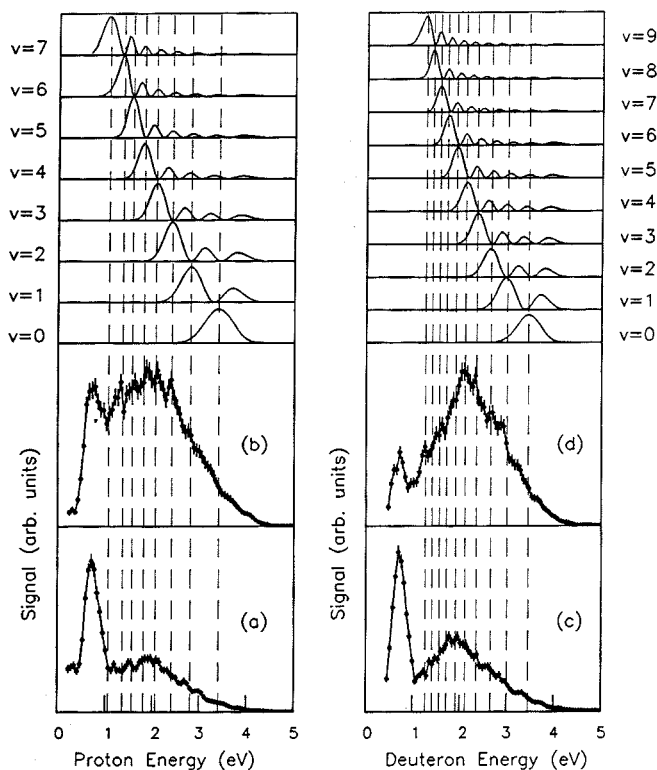

Figure 12   Kinetic energy spectra of protons and deuterons from the 769-nm photodissociation of H_2^+ (*left*) and D_2^+ (*right*) at 1 PW/cm^2 (*a, c*) and 2 PW/cm^2 (*b, d*). The Franck-Condon overlaps between the light-induced bound state and the repulsive Coulomb state form a series of maxima separated by the same interval as the modulations in the spectra. [From Zavriyev et al (13).]
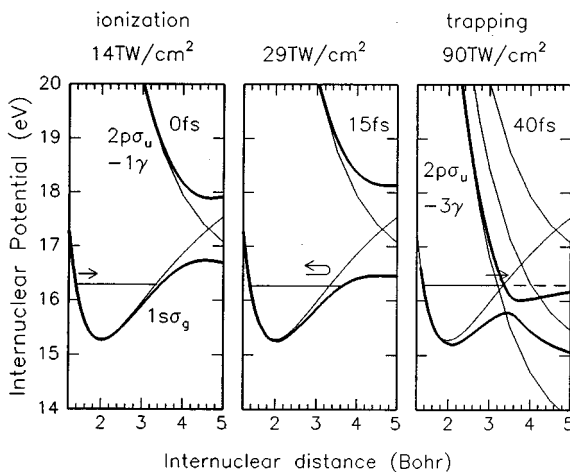
Figure 13 Evolution of the adiabatic potential curves for the $1s\sigma_g$ and $2p\sigma_u$ states of H_2^+ at various times in a given laser pulse, illustrating a possible scenario in which population might become trapped in a light-induced adiabatic well (see text). [From Zavriyev et al (13).]

where the intensity falls below the point that the adiabatic well can support bound states. This effect may be important in the dynamics of the Coulomb explosion.

Coulomb Explosion

The remaining electron in H_2^+ can be promoted directly to the continuum, and in larger molecules, multiple electrons can be removed during the dissociation process. Frasinski et al (8) proposed that multiple ionization occurs quickly enough, while the nuclei are still at or near their equilibrium separation, that the ionic fragments acquire large kinetic energies from the resultant Coulomb repulsion. The dynamics of these Coulomb explosion dissociations were the subject of an excellent review in 1993 (53), to which the reader is referred. We briefly cover the field-ionization model, which is more fully reviewed in Reference 53, in order to discuss work that has been done in the field since that review.

The tunneling model as applied to molecules was described qualitatively in the introduction. A more detailed model of the stepwise ionization with increasing nuclear separation was formulated by Brewczyk & Frasinski (54). Their Thomas-Fermi-Dirac (TFD) model, a generalization of the Thomas-Fermi model that includes the electron exchange energy, treats the electrons as a continuous charge distribution. In Figure 14, the potential for a diatomic

molecule, N_2, along the internuclear axis is plotted for three different internuclear distances. The shaded region, representing the electron cloud, fills the potential wells up to the Fermi energy. As the optical electric field oscillates, the asymptotic slope of the curve changes from positive to negative, and electron transfer occurs both out of the wells into the continuum (ionization), and back and forth between the wells. Note that charge can escape not only by tunneling through the left or right potential barrier, but also through the internal barrier directly to the continuum, when both the field and the Fermi energy in the "uphill" well are large enough. Once loss to the continuum has occurred, both charge centers have a net positive charge, and the Coulomb repulsion drives them further apart. As the internuclear separation increases, the internal barrier grows higher; for a given field, there is a separation beyond which tunneling through the internal barrier is suppressed. The Coulomb repulsion between the remaining charge cores, after ionization has ceased, determines the final ion energies.

Figure 15 illustrates Brewczyk & Frasinski's calculated evolution of the dissociation of a nitrogen molecule in laser pulses of different peak field strengths (a 10.3 V/Å peak field corresponds to an intensity of 5×10^{15} W/cm^2). The full curves represent the ionization level of the minimally ionized molecule as a function of internuclear separation. The molecule is minimally ionized when the Fermi level just reaches the top of the barrier. The path described by the dotted line shows the evolution of the molecule suddenly exposed to an optical field with a peak 10.3 V/Å field. At the first crest, while the nuclei are still at their equilibrium separation, the molecule rapidly ionizes to a charge slightly greater than $+3$. Coulomb repulsion then begins to drive the ions apart, and on each oscillation of the field, slightly more charge is removed until, shortly
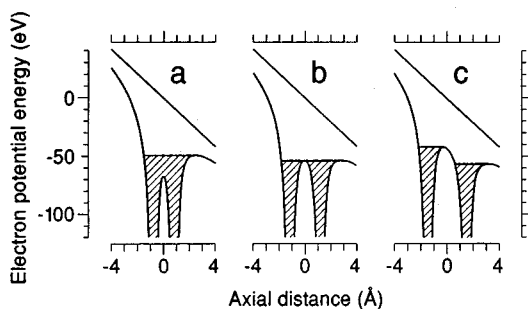

Figure 14   TFD potential energy on the axis of a nitrogen molecule in a 10.3 V/Å electric field parallel to the molecular axis, at internuclear separations of (*a*) 1.6 Å, (*b*) 2.3 Å (dissociation point), and (*c*) 3.0 Å. [From Brewczyk & Frasinski (54).]
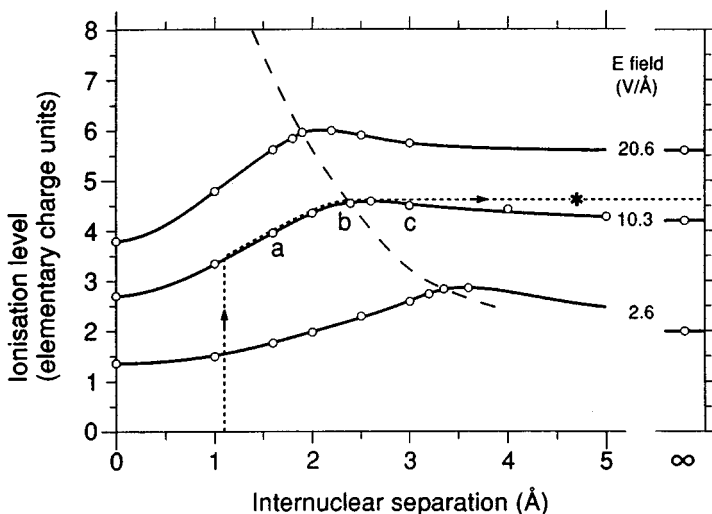
Figure 15   Ionization level of a nitrogen molecule as a function of internuclear separation in the TFD model, for several electric field values. The dotted line shows the evolution of the ionization of a molecule suddenly exposed to a 10.3 V/Å field. The points *a, b, c* correspond to the panels of Figure 14. The dashed curve indicates the dissociation point, and the star indicates the separation past which charge transfer between the ions is inhibited. [From Brewczyk & Frasinski (54).]

after the dissociation point (marked in the figure by the long-dashed curve), the point of maximum ionization is reached. The ions continue to move apart with no further charge loss. Charge transfer between the two ions continues to occur up to the separation marked on the graph by a star, the direction of transfer changing on each half-oscillation of the field.

The TFD model has some notable successes but raises difficulties as well. It predicts the highest ionization stage of dissociation as a function of laser intensity reasonably well, although thresholds for ionization stages below $+3$ are underestimated by the theory. It also explains the experimentally observed predominance of symmetric fragmentation (i.e. dissociation fragments differing in charge state by one unit of charge or less). The alternating direction of charge transfer beyond the dissociation point serves to equalize the remaining charge between the ions. Most importantly, the field-dependent maximum in the full curves at an internuclear separation greater than R_e is consistent with Codling's suggestion (55) that, for a given field, there is an optimal internuclear separation that maximizes the ionization of a molecule. This accounts qualitatively for the experimental observation (56) that the total energy of dissociation fragments is lower than the Coulomb energy at the equilibrium internuclear separation.

Lower-charge states, being formed at smaller internuclear separations, should more closely approximate the Coulomb energy at R_e than higher-charge states. However, recent experiments by Schmidt et al (10) in Cl_2 have shown that the ratio E_{exp}/E_c is the same for all fragmentation channels of the molecule, up to charge states of $+8$. They also analyzed previous experiments on seven other molecules and found that E_{exp}/E_c is closely correlated with the equilibrium internuclear separation, with shorter bonds yielding lower values than longer bonds. For chlorine, $R_e = 2.0$ Å, and $E_{exp}/E_c = 70\%$, while for H_2, CO, N_2, O_2, C_2H_2, and CO_2, all of which have bond lengths between 1.1 and 1.2 Å, E_{exp}/E_c lies between 40 and 50%. If an effective separation R_{eff} is defined to be the separation at which Coulomb repulsion would produce the observed fragment energies, then there is an empirical scaling $R_{eff} = a\sqrt{R_e}$, with $a \approx 2.3$ being independent of the molecule. The picture that emerges then is one of the molecule being stretched to an optimal length at which rapid ionization branching among various charge states is followed by Coulomb repulsion of the charged fragments.

A more surprising finding is that both the branching ratios among fragmentation channels and the fragment kinetic energies are independent of laser wavelength and pulse duration (10, 17). A short pulse (< 100 fs) would be expected to produce higher-energy fragments, the internuclear separation being essentially restricted near R_e during the pulse rise time and yielding more ionization at smaller R. The long-pulse data yield yet another surprise. Dissociation occurring during and shortly after the pulse rise should lead to further ionization of the dissociation fragments during the remainder of the pulse, yet none is observed (10, 17). The absence of this postdissociation ionization is not simply due to a low atomic ionization cross section; this has been recently demonstrated in a pump-probe experiment by Schmidt et al (18). It appears then that the molecule does not dissociate early in the pulse, but is somehow transiently stabilized during the greater part of the pulse and dissociates near the end.

Theoretical time-dependent studies (14–16, 57) have yielded some understanding of the fact that the Coulomb explosion occurs at some optimal R_{eff} greater than R_e. Ionization enhancement of the molecule at an optimal internuclear distance is actually present in the TFD model, but its magnitude is underestimated because of the assumption that the electron cloud follows the oscillations of the field adiabatically. The time-dependent studies have shown that the nonadiabatic population of the "uphill" potential well (see Figure 14) leads to ionization rates an order of magnitude larger than those of the neutral atom. The range of R_{eff} at which this enhancement occurs is consistent with the experimental values and shows the same insensitivity to laser parameters as the experiments.

Some stabilization of the molecule against dissociation has also been predicted by the time-dependent calculations on molecular hydrogen (16), with lifetimes of a few tens of femtoseconds. A more detailed physical picture has recently been proposed by Viel et al (19). The Coulomb repulsion in their model is overcome by a laser-induced cloud of electrons between the nuclei. They consider the problem in a frame moving with the electrons, oscillating under the combined fields of the laser and the ion cores, analogous to the use of the Kramers-Henneberger transformation in the study of atomic stabilization (58). The ground state of the time-averaged Hamiltonian in this frame is the stabilizing state. The electron energy surfaces are obtained by numerically solving the time-dependent Schrödinger equation, and a variational approach is used to calculate the actual electron trajectory. Viel et al find that stable states with lifetimes in the range of 10 ps exist and are characterized by the electron spending most of its time near one of the nuclei and jumping between them when the field is small. The range of R for such states, 4–5 bohr, is in very good agreement with the experimentally determined values of R_{eff}.

Many puzzles remain in the dynamics of multiple electron dissociative ionization. Though the plausibility of stabilization has been demonstrated, more detailed calculations need to be performed, and an understanding of the dynamics of the loading of the molecule into the stabilized state has yet to be found. It is unclear how the molecule survives the laser pulse turn-on and how the stabilization process competes with the ionization enhancement discussed above.

COHERENT CONTROL OF DISSOCIATION USING A TWO-COLOR FIELD

In 1988, Shapiro et al (59) demonstrated theoretically that manipulating the relative phase between two harmonic optical fields was sufficient to coherently control the branching ratios between exit channels in some molecular photodissociation processes. The experimental demonstration has proven to be more difficult, but important steps have been made. Atomic experiments have demonstrated the modulation of both photoelectron yield (via an interference in a bound-bound transition probability) (60, 61) and angular distribution (62–65). Phase-dependent photoelectron yields have also been observed in a two-color molecular experiment (66).

Sheehy et al (67) recently demonstrated the first use of the relative phase to control the fragment distribution in a photodissociation process. The two-color field consists of the 1053-nm fundamental of a regeneratively amplified Nd:YLF mode-locked laser (50 ps FWHM pulsewidth) and its second harmonic. The relative phase ϕ between the two colors is well defined by the doubling

process and is subsequently varied by varying the length of dispersive material that the beam traverses. The time dependence of the optical electric field $E = E_1 \cos(\omega t) + E_2 \cos(2\omega t + \phi)$ is shown in the insets of Figure 16 for $\phi = 0$, 0.6π, and π, with $E_1 = E_2$. Note that the extrema have different magnitudes in the positive and negative directions and that the size of the asymmetry is a function of ϕ. The figure also shows the time-of-flight (TOF) spectrum produced in the photodissociation of HD^+, which is expanded about the H^+ and D^+ arrival peaks. In the interaction region, a small dc field reverses the velocity of ions emitted in the backward direction (away from the detector), which then arrive at the detector with an energy-dependent delay relative to the forward ions, yielding the double-peak structures in the figure (the center peak of the D^+ is due to residual H_2^+). There is a marked forward-to-backward asymmetry in both isotopes, which mirrors the forward-to-backward asymmetry in the optical electric field. This is more clearly shown in Figure 17a, where the
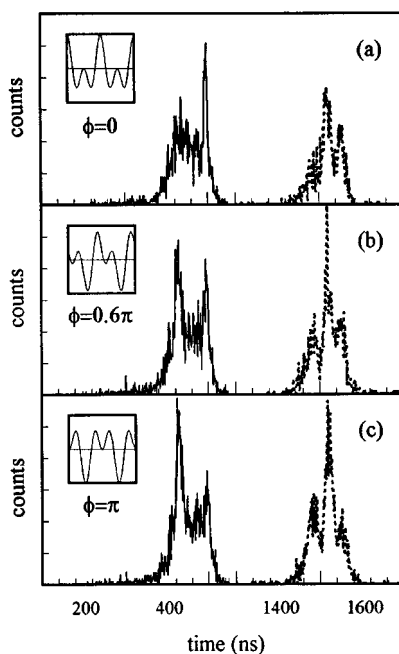

Figure 16   Time of flight spectra expanded about the H^+ (*solid*) and D^+ (*dashed*) arrival peaks for (*a*) $\phi = 0$, (*b*) $\phi = 0.6\pi$, and (*c*) $\phi = \pi$. The optical electric field is plotted over two optical cycles in the inset of each graph for the corresponding value of the two-color relative phase ϕ. The dissociation fraction is 0.12. The total intensity is 2×10^{13} W/cm^2.
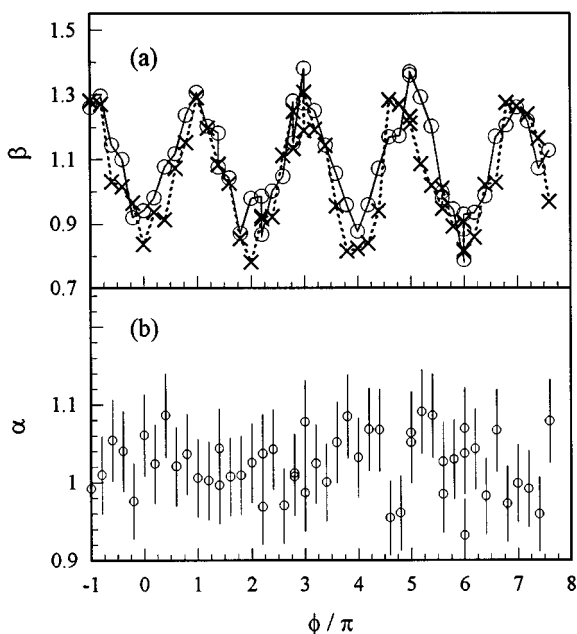
Figure 17 (*a*) The yield ratios $\beta = \frac{\text{forward yield}}{\text{backward yield}}$ of H^+(*circles*) and D^+ (*crosses*) vs the relative two-color phase ϕ in the dissociation of HD^+. (*b*) The degree of spatial separation of the H^+ and D^+ fragments, $\alpha = \sqrt{\frac{\beta_{H+}}{\beta_{D+}}}$, vs ϕ. The uncertainty is indicated by the error bars.

ratios of forward-to-backward yields for each isotope, β_{H+} and β_{D+}, are plotted as a function of ϕ over several cycles. Modulation depths as large as 70% are observed. The phase-dependent asymmetry of protons in the photodissociation of H_2^+ behaves in the same way.

This spatial asymmetry arises from an interference between absorption from and stimulated emission into the two laser fields and is well modeled by time-dependent calculations (68, 69). Calculations on the HD^+ ion predict that a selectivity between dissociation along the nearly degenerate $1s\sigma_g$ and $2p\sigma_u$ electronic surfaces is possible (70). In H_2^+, these states are degenerate at large internuclear distances, but the degeneracy is lifted in the heteronuclear case, as the nuclear mass difference couples the electronic and nuclear motions. The asymptotic limits are separated by 29.8 cm^{-1} and correspond to distinct dissociation products: $D + H^+$ and $H + D^+$. The mixing of states of opposite symmetry means that rovibrational transitions within each electronic state are dipole allowed, and interferences between interelectronic and intraelectronic

transitions become important. The products of the two dissociation channels can then be spatially separated through the adjustment of the relative phase of a two-color field. The effect becomes important only at longer wavelengths (peaking near 10 μm), at which the larger number of photons required for dissociation assures that the asymptotic region, where the dipole moments of each electronic state become large, is sampled. In the experiment using a 1053-nm fundamental wavelength, the effect is negligible (Figure 17*b*).

SUMMARY

Short-pulse lasers have evolved into an extremely versatile tool in physical chemistry. They have opened the frontier to a new dynamical regime, changed the way that we look at molecular dynamics, and may ultimately permit chemical manipulation at the level of the molecular wavefunction.

The high intensities attainable with short-pulse lasers have permitted the first exploration of the physics of atoms and molecules in optical fields comparable to Coulomb binding fields. We have seen that relatively simple semiclassical models provide a good intuitive understanding of many of the new atomic phenomena in this regime, with some important limitations. Quantum calculations have completed the picture for most of these limitations, but the problem of correlated two-electron emission remains a puzzle, which may require a full two-electron quantum-mechanical calculation to solve.

Molecular studies in strong fields have also uncovered a host of new phenomena, e.g. bond softening, ATD, vibrational trapping, and Coulomb explosions. Most of these phenomena are well understood only by treating the light and molecule together as a single quantum system. It is the presence of states induced by the light field that makes the dynamics so interesting. Vibrational trapping and the dynamics of Coulomb explosions are also both examples of how short-pulse lasers are affording us an understanding of molecular dynamics at time scales of tens of femtoseconds or less.

Perhaps the greatest promise lies in the field of coherent optimal control, which is still very much in its infancy. The possibility of manipulating the optical interaction, and through it the evolution of the molecular wavefunction, on femtosecond time scales is now very close to realization. Short-pulse technology may ultimately contribute to the fulfillment of the chemist's dream of engineering molecules one atom at a time.

Literature Cited

1. Agostini P, Fabre G, Petite G, Rahman NK. 1979. *Phys. Rev. Lett.* 42:1127–30
2. DiMauro LF, Agostini P. 1995. *Adv. Atomic Mol. Opt. Phys.* 35:79–120
3. Walker B, Sheehy B, DiMauro LF, Agostini P, Schafer KJ, Kulander KC. 1994. *Phys. Rev. Lett.* 73:1227–30
4. Augst S, Talebpour A, Chin SL, Beaudoin Y, Chaker M. 1995. *Phys. Rev. A* 52:R917–19
5. van Linden van der Heuvell HB, Muller HG. 1988. In *Multiphoton Processes,* ed. SJ Smith, PL Knight. London: Cambridge Univ. Press
6. Schafer KJ, Yang B, DiMauro LF, Kulander KC. 1993. *Phys. Rev. Lett.* 70:1599–602
7. Corkum P. 1993. *Phys. Rev. Lett.* 71:1994–97
8. Frasinski LJ, Codling K, Hatherly P, Barr J, Ross IN, Toner WT. 1987. *Phys. Rev. Lett.* 58:2424–27
9. Frasinski LJ, Codling K, Hatherly PA. 1989. *Science* 246:1029–31
10. Schmidt M, Normand D, Cornaggia C. 1994. *Phys. Rev. A* 50:5037–45
11. Bucksbaum PH, Zavriyev A, Muller HG, Schumacher DW. 1990. *Phys. Rev. Lett.* 64:1883–86
12. Zavriyev A, Bucksbaum PH, Muller HG, Schumacher DW. 1990. *Phys. Rev. A* 42:5500–13
13. Zavriyev A, Bucksbaum PH, Squier J, Saline F. 1993. *Phys. Rev. Lett.* 70:1077–81
14. Seideman T, Ivanov MY, Corkum PB. 1995. *Phys. Rev. Lett.* 75:2819–22
15. Zuo T, Bandrauk AD. 1995. *Phys. Rev. A* 52:R2511–14
16. Chelkowski S, Zuo T, Atabek O, Bandrauk AD. 1995. *Phys. Rev. A* 52:2977–83
17. Normand D, Schmidt M. 1996. *Phys. Rev. A.* 53:R1958–61
18. Schmidt M, Normand D, Lewenstein M, D'Oliveira P. 1996. *Phys. Rev. A.* Submitted
19. Viel A, Lewenstein M, Normand D, Schmidt M, Cirac JI. 1996. *Phys. Rev. Lett.* Submitted
20. Peirce AP, Dahleh A, Rabitz H. 1988. *Phys. Rev. A* 37:4950–64
21. Kohler B, Krause JL, Raksi F, Wilson KR, Yakovlev VV, et al. 1995. *Acc. Chem. Res.* 28:133–40
22. Kulander KC. 1988. *Phys. Rev. A* 38:778–87
23. Ammosov MV, Delone NB, Krainov VP. 1986. *Sov. Phys. JETP* 64:1191–94
24. L'Huillier A, Schafer KJ, Kulander KC. 1991. *J. Phys. B* 24:3315–41
25. Krause JL, Schafer KJ, Kulander KC. 1992. *Phys. Rev. Lett.* 68:3535–38
26. Yang B, Schafer KJ, Walker B, Kulander KC, Agostini P, DiMauro LF. 1993. *Phys. Rev. Lett.* 71:3770–73
27. Lewenstein M, Kulander KC, Schafer KJ, Bucksbaum PH. 1995. *Phys. Rev. A* 51:1495–507
28. Schafer KJ, Kulander KC. 1994. In *Proc. St. Malo Conf. High Field Interactions and Short Wavelength Generation, Tech. Dig.* 16:98–100. Washington, DC: Opt. Soc. Am.
29. Cohen S, Camus P, Bolovinos A. 1993. *J. Phys. B* 26:3783
30. L'Huillier A, Lompre LA, Mainfray G, Manus C. 1983. *Phys. Rev. A* 27:2503–12
31. Walker B, Mevel E, Yang B, Breger P, Chambaret JP, et al. 1993. *Phys. Rev. A* 48:R894–97
32. Charalambidis D, Lambropoulos P, Schröder H, Faucher O, Xu H, et al. 1994. *Phys. Rev. A* 50:R2822–25
33. Fittinghoff DN, Bolton PR, Chang B, Kulander KC. 1992. *Phys. Rev. Lett.* 69:2642–45

34. Wehlitz R, Heiser F, Hemmers O, Langer B, Menzel A, Becker U. 1991. *Phys. Rev. Lett.* 67:3764–67
35. Giusti-Suzor A, Mies FH, DiMauro LF, Charron E, Yang B. 1994. *J. Phys. B* 27:1–31
36. Yang B, Saeed M, DiMauro LF, Zavriyev A, Bucksbaum PH. 1991. *Phys. Rev. A* 44:R1458–61
37. Normand D, Lompre LA, Cornaggia C. 1992. *J. Phys. B* 25:L497–503
38. Chu S-I. 1981. *J. Chem. Phys.* 75:2215–21
39. Chu S-I. 1991. *J. Chem. Phys.* 94:7901–9
40. Muller HG. 1992. In *Coherence Phenomena in Atoms and Molecules in Laser Fields*, NATO ASI Ser. B, ed. AD Bandrauk, SC Wallace, 316:89. New York: Plenum
41. Giusti-Suzor A, He X, Atabek O, Mies FH. 1990. *Phys. Rev. Lett.* 64:515–18
42. Giusti-Suzor A, Mies FH. 1992. *Phys. Rev. Lett.* 68:3869–72
43. Yao G, Chu S-I. 1992. *Chem. Phys. Lett.* 197:413–18
44. Yao G, Chu S-I. 1993. *Phys. Rev. A* 48:485–94
45. Aubanel EE, Gauthier JM, Bandrauk AD. 1993. *Phys. Rev. A* 48:2145–52
46. Aubanel EE, Conjusteau A, Bandrauk AD. 1993. *Phys. Rev. A* 48:R4011–14
47. Fedorov MV, Kudrevatova OV, Makarov VP, Samokhin AA. 1975. *Opt. Commun.* 13:299
48. Yuan M, George TF. 1978. *J. Chem. Phys.* 68:3040–52
49. Bandrauk AD, Sink ML. 1981. *J. Chem. Phys.* 74:1110–17
50. Freeman RR, Bucksbaum PH, Milchberg H, Darack S, Schumacher D, Geusic ME. 1987. *Phys. Rev. Lett.* 59:1092–95
51. Gibson GN, Freeman RR, McIlrath TJ. 1991. *Phys. Rev. Lett.* 67:1230–33
52. Helm H, Dyer MJ, Bissantz H. 1991. *Phys. Rev. Lett.* 67:1234–37
53. Codling K, Frasinski LJ. 1993. *J. Phys. B* 26:783–809
54. Brewczyk M, Frasinski LJ. 1991. *J. Phys. B* 24:L307–13
55. Codling K, Frasinski LJ, Hatherly PA. 1989. *J. Phys. B* 22:L321–27
56. Codling K, Frasinski LJ, Hatherly P, Barr JRM. 1987. *J. Phys. B* 20:L525–31
57. Posthumus JH, Frasinski LJ, Giles AJ, Codling K. 1995. *J. Phys. B* 28:L349–53
58. Pont M, Gavrila M. 1990. *Phys. Rev. Lett.* 65:2362–65
59. Shapiro M, Hepburn JW, Brumer P. 1988. *Chem. Phys. Lett.* 149:451
60. Chen CE, Yin Y-Y, Elliott DS. 1990. *Phys. Rev. Lett.* 64:507–10
61. Chen CE, Elliott DS. 1990. *Phys. Rev. Lett.* 65:1737–40
62. Muller HG, Bucksbaum PH, Schumacher DW, Zavriyev A. 1990. *J. Phys. B* 23:2761–69
63. Yin Y-Y, Chen CE, Elliott DS, Smith AV. 1992. *Phys. Rev. Lett.* 69:2353–56
64. Baranova NB, Beterov IM, Zel'dovich BY, Ryabtsev II, Chudinov AN, Shul'ginov AA. 1992. *JETP Lett.* 55:439–44
65. Schumacher DW, Weihe F, Muller HG, Bucksbaum PH. 1994. *Phys. Rev. Lett.* 73:1344–47
66. Park SM, Lu S-P, Gordon RJ. 1991. *J. Chem. Phys.* 94:8622–24
67. Sheehy B, Walker B, DiMauro LF. 1995. *Phys. Rev. Lett.* 74:4799–802
68. Charron E, Giusti-Suzor A, Mies FH. 1993. *Phys. Rev. Lett.* 71:692–95
69. Charron E, Giusti-Suzor A, Mies FH. 1994. *Phys. Rev. A* 49:R641–44
70. Charron E, Giusti-Suzor A, Mies FH. 1995. *Phys. Rev. Lett.* 75:2815–18